Photonics-Based Instantaneous Microwave Frequency Measurement System With Improved Resolution and Robust Performance

Henghao Chen, Chongjia Huang, and Erwin H. W. Chan, *Senior Member, IEEE*

***Abstract*—This paper presents a photonics-based instantaneous microwave frequency measurement system. The system operates based on the frequency-to-power mapping technique. The trade-off between frequency measurement range and resolution, which is present in the reported frequency-to-power-mapping based frequency measurement systems, is addressed by designing the system to produce two amplitude comparison functions (ACFs). Using two ACFs enables an RF signal frequency in a specified range to be determined while having an improved resolution and smaller errors compared to using only one ACF for frequency measurement. The proposed frequency measurement system is designed to have a simple structure and robust performance suitable for use in real world applications. The effect of the higher order sidebands and harmonics on the system performance are investigated. Proof-of-concept experiments are carried out with results showing frequency measurement errors can be reduced by using the proposed system that generates two ACFs for frequency measurement.**

***Index Terms*—Instantaneous frequency measurement, frequency-to-power mapping, amplitude comparison function, microwave measurement.**

I. Introduction

MICROWAVE frequency measurement is a topic of interest in the microwave photonics community. This is because microwave photonics can provide solutions to overcome limitations such as limited frequency measurement range and to solve problems such as electromagnetic interference, present in conventional electronics-based frequency measurement systems. Numerous photonics-based frequency measurement systems have been reported [1], [2], [3]. Their operation principles can be classified into three catalogues, which are frequency-to-power mapping, frequency-to-space mapping, and frequency-to-time mapping. Among them, the systems based on the frequency-to-power mapping technique, in general, have a simpler structure and a faster measurement time compared to the other two techniques. Majority of the frequency-to-power-mapping based frequency measurement systems are based on generating two output RF signals with different frequency characteristics, which are used to produce an amplitude comparison function (ACF). The frequency of an unknown input RF signal can be determined according to a unique power ratio and frequency relationship in the ACF. For a frequency measurement system to be used in practice, it needs to have a simple structure and a robust performance. The reported frequency-to-power-mapping based frequency measurement systems have the drawbacks of requiring different-wavelength laser sources [4], multiple optical modulators [5], multiple dispersive mediums [6], specially designed components such as photonic crystal nanocavities [7], or electrical components such as a power divider [8] that limits the frequency measurement range. The frequency-to-power-mapping based frequency measurement systems reported in [9], [10], [11] have an all-optical, single-laser and single-modulator structure. However, they have stability issues. For example, a change in environmental condition causes change in the light polarisation state or the transfer function of a component used in the system, which leads to errors in frequency measurement.

In this paper, we present an instantaneous microwave frequency measurement system implemented using the frequency-to-power mapping technique. It has a simple structure and a robust performance. Additionally, it has the novelty of being capable of producing two ACFs for increasing frequency measurement resolution and reducing frequency measurement errors. The system can be designed to focus on frequency measurement in a specified frequency range while having an improved resolution. The paper is organised as follows. The topology and the operation principle of the proposed frequency measurement system are presented in Section II. This section also presents the investigation on the effects of higher order sidebands and harmonics on the system performance. Section III describes an extension of the proposed structure that produces two ACFs for improving the frequency measurement resolution. Proof of concept experiments for one-ACF and two-ACF based frequency measurement systems are conducted and the results are presented in Section IV. Finally, conclusions are given in Section V.

II. Topology and Operation Principle

Fig. 1 shows the structure of the proposed photonics-based instantaneous microwave frequency measurement system. A continuous wave (CW) light from a laser source is launched into an optical phase modulator (PM) driven by an RF signal

Manuscript received 25 August 2022; revised 29 September 2022; accepted 3 October 2022. Date of publication 10 October 2022; date of current version 13 October 2022. *(Corresponding author: Erwin H. W. Chan.)*

The authors are with the College of Engineering, IT and Environment, Charles Darwin University, Darwin, NT 0909, Australia (e-mail: chhcnau@gmail.com; 1286660746@qq.com; erwin.chan@cdu.edu.au).

Digital Object Identifier 10.1109/JPHOT.2022.3212709

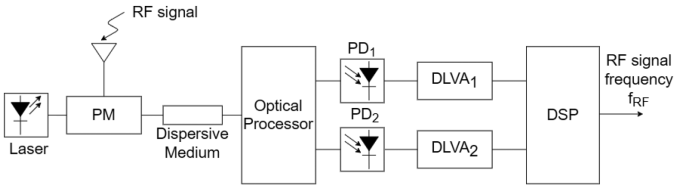

Fig. 1. Structure of the proposed photonics-based instantaneous microwave frequency measurement system.

with an unknown frequency f_{RF} received by an antenna. The PM output electric field is given by

$$E_{PM,out}(t) = E_{in}\sqrt{t_{ff}}e^{j\omega_c t} \times \left[J_0(m)+J_1(m)e^{j\omega_{RF}t} - J_1(m)e^{-j\omega_{RF}t}\right] \quad (1)$$

where E_{in} is the electric field amplitude of the CW light into the PM, t_{ff} is the PM insertion loss, ω_c is the angular frequency of the CW light into the PM, $J_n(x)$ is the Bessel function of nth order of the first kind, $m = \pi V_{RF}/V_\pi$ is the modulation index, V_{RF} is the amplitude of the RF signal into the modulator, V_π is the switching voltage of the PM and $\omega_{RF} = 2\pi f_{RF}$ is the angular frequency of the input RF signal. The RF phase modulated optical signal passes through a dispersive medium, which can be a length of standard single mode fibre (SMF) or a length of dispersion compensating fibre (DCF). A phase shift is introduced to the upper and lower first order sidebands relative to the optical carrier and is given by [12]

$$\theta\left(f_{RF}\right) = \pi \cdot D \cdot \frac{\lambda_c^2}{c} \cdot L \cdot f_{RF}^2 \quad (2)$$

where D is the dispersion parameter, λ_c is the wavelength of the CW light into the PM, c is the speed of light in vacuum and L is the length of a standard SMF or a DCF used as a dispersive medium. The output of the dispersive medium is connected to a liquid crystal on silicon (LCOS) based optical processor, which is programmed to introduce a phase shift α_N to the optical carrier at the optical processor output Port N where $N = 1$ or 2. Therefore, the electric field at the optical processor output Port N can be written as

$$E_{out,N}(t) = \frac{1}{\sqrt{2}}E_{in}\sqrt{t_{ff}}\sqrt{l_o}e^{j\omega_c t} \times \left[e^{j\alpha_N}J_0(m)+e^{j\theta(f_{RF})}(J_1(m)e^{j\omega_{RF}t} - J_1(m)e^{-j\omega_{RF}t})\right] \quad (3)$$

where l_o is the overall insertion loss of the dispersive medium and the LCOS based optical processor. The two system output optical signals are detected by photodetectors (PD_1 and PD_2). A photocurrent, which is the product of the PD responsivity $\Re$ and the absolute square of the system output electric field, is generated after photodetection. The amplitude of the photocurrent at the RF signal frequency at the output of PD_N is given by

$$I_{RF,N}\left(f_{RF}\right) = -2\Re P_{in}t_{ff}l_o J_0(m)J_1(m) \times \sin\left(\theta\left(f_{RF}\right) - \alpha_N\right) \quad (4)$$

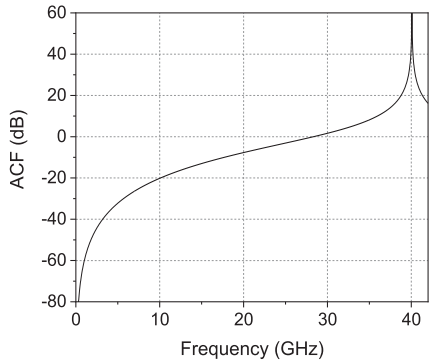

Fig. 2. ACF of the proposed photonics-based instantaneous microwave frequency measurement system operated under small signal modulation condition.

where P_{in} is the power of the CW light into the PM. A microwave power meter can be used to measure the PD output RF signal power [8], which is proportional to the square of the amplitude of the output RF signal photocurrent. The frequency of the RF signal into the system can be determined from the ratio of the two PD output RF signal powers, i.e., the ACF. The ACF can also be obtained by using a detector logarithmic video amplifier (DLVA) [1] connected to the PD output as shown in Fig. 1. A DLVA is formed by a Schottky diode detector followed by a logarithmic video amplifier. The Schottky diode detector converts an input RF signal power into a DC voltage, which is then amplified by an amplifier with a logarithmic transfer function. The DLVA output DC voltage has a linear relationship with the DLVA input RF signal power in the unit of dBm. Since the ACF is the ratio of the two PD output RF signal powers, the ACF in the unit of decibel can be obtained by simply dividing the difference of the two DLVA output DC voltages by the slope of the DLVA transfer function, i.e.,

$$ACF\left(f_{RF}\right) = \frac{V_{o,DLVA2} - V_{o,DLVA1}}{DLVA\ Slope} = 20\log_{10}\left[\sin\left(\theta\left(f_{RF}\right) - \alpha_2\right)\right] - 20\log_{10}\left[\sin\left(\theta\left(f_{RF}\right) - \alpha_1\right)\right] \quad (5)$$

where $V_{o,DLVAN}$ is the DC voltage at the output of $DLVA_N$. These subtraction and division operation are performed in a digital signal processor (DSP) connected to the DLVA outputs. As shown in (5), the ACF becomes $\tan^2\theta\left(f_{RF}\right)$ when a phase shift of $\alpha_1 = 0°$ and $\alpha_2 = -90°$ are introduced to the optical carriers at the two optical processor output ports. According to (2), the phase shift $\theta\left(f_{RF}\right)$ is proportional to the square of the RF signal frequency f_{RF}. Hence the system input RF signal frequency can be determined based on the value of the ACF via a look-up table implemented using (2) and (5). Fig. 2 shows a one-to-one mapping between an ACF value and an RF signal frequency over a frequency range of 0 to 40 GHz, when a 2.43 km long standard SMF with a dispersion parameter of 16 ps/nm·km is used as the dispersive medium in the proposed structure. It can be seen from (5) that the ACF is independent of the modulation index. Hence the RF signal frequency can be determined from the ACF without knowing the input RF signal power.

Note that, as in most reported photonics-based frequency measurement systems [6], [8], [11], the above analysis assumes the system is operated under small signal modulation condition and hence only the first order modulation sidebands are included in the analysis. However, in practice, the input RF signal power may not be small and may not be known prior to frequency measurement. The analysis of the frequency measurement system shown in Fig. 1 was repeated with the inclusion of the second and third order modulation sidebands. The electric field at the LCOS based optical processor output Port *N* becomes

$$\begin{aligned} E_{out,N}(t) = \frac{1}{\sqrt{2}} E_{in}\sqrt{t_{ff}}\sqrt{l_o}e^{j\omega_c t}\left[e^{j\alpha_N}J_0(m)\right. \\ + e^{j\theta(f_{RF})}\left(J_1(m)e^{j\omega_{RF}t} - J_1(m)e^{-j\omega_{RF}t}\right) \\ + e^{j4\theta(f_{RF})}\left(J_2(m)e^{j2\omega_{RF}t} + J_2(m)e^{-j2\omega_{RF}t}\right) \\ \left. + e^{j9\theta(f_{RF})}\left(J_3(m)e^{j3\omega_{RF}t} - J_3(m)e^{-j3\omega_{RF}t}\right)\right] \end{aligned} \tag{6}$$

Beating between the first and second order sidebands and the beating between the second and third order sidebands at the PD also generate a photocurrent at the RF signal frequency. Therefore, the amplitude of the photocurrent at the RF signal frequency at the output of PD_N is given by

$$\begin{aligned} I_{RF,N}(f_{RF}) = & -2\Re P_{in}t_{ff}l_o\left[J_0(m)J_1(m)\right. \\ & \times \sin\left(\theta\left(f_{RF}\right) - \alpha_N\right) \\ & + J_1(m)J_2(m)\sin\left(3\theta\left(f_{RF}\right)\right) \\ & \left. + J_2(m)J_3(m)\sin\left(5\theta\left(f_{RF}\right)\right)\right] \end{aligned} \tag{7}$$

As in many reported photonics-based frequency measurement systems, the proposed structure shown in Fig. 1 generates harmonic components, which are also detected by the Schottky diode detector in the DLVA. The amplitude of the photocurrent at the second order harmonic RF signal frequency at the output of PD_N can be obtained from (6) and is given by

$$\begin{aligned} I_{2RF,N}(f_{RF}) = & 2\Re P_{in}t_{ff}l_o\left[J_0(m)J_2(m)\right. \\ & \times \cos\left(4\theta\left(f_{RF}\right) - \alpha_N\right) \\ & \left. + J_1(m)J_3(m)\cos\left(8\theta\left(f_{RF}\right)\right) - J_1^2(m)/2\right] \end{aligned} \tag{8}$$

The voltage produced by the DLVA is proportional to the sum of the output fundamental and second order harmonic RF signal power. Hence, after including the second and third order sidebands and the second order harmonics in the analysis, the ACF becomes

$$\begin{aligned} ACF(f_{RF}) &= \frac{V_{o,DLVA2} - V_{o,DLVA1}}{DLVASlope} \\ &= 10\log_{10}\left[I_{RF,2}^2(f_{RF}) + I_{2RF,2}^2(f_{RF})\right] \\ &\quad - 10\log_{10}\left[I_{RF,1}^2(f_{RF}) + I_{2RF,1}^2(f_{RF})\right] \end{aligned} \tag{9}$$

Equations (7)–(9) indicate that the ACF is dependent on the modulation index, which is in turn dependent on the power of the RF signal into the system. Fig. 3(a) plots the ACFs for different modulation indexes of 0.1, 0.3 and 0.5. Changing the modulation index from 0.1 to 0.5 corresponds to the input RF signal power changes from −7.9 dBm to 6.4 dBm for a PM having a switching voltage of 4 V. Fig. 3(a) shows the ACFs have a large difference at around the peak of the ACF. Note that the Schottky diode detector in the DLVA also detects the powers of the third and higher order harmonic components and the noise components in the system. This causes the ACF value to deviate from the simulation result shown in Fig. 3(a) at around the dip of the ACF. Therefore, the dispersive medium needs to be designed to ensure the peak and the dip of the ACF are outside the frequency measurement range. Hence, the input RF signal frequency can be determined with little errors, using an ACF value obtained from the output RF signal powers and a look-up table implemented using (9) with a fixed modulation index of for example 0.3, without knowing the power of the RF signal into the system.

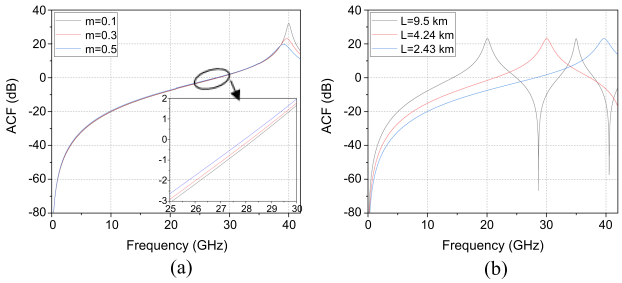

Fig. 3. ACFs of the proposed photonics-based instantaneous microwave frequency measurement system for (a) different modulation indexes while the SMF length *L* is fixed at 2.43 km, and (b) different SMF lengths while the modulation index *m* is fixed at 0.3. The phase shifts introduced to the optical carriers at the two optical processor output ports are $\alpha_1 = 0°$ and $\alpha_2 = -90°$.

Frequency measurement resolution, which is an important figure of merit in a frequency measurement system, is dependent on the slope of an ACF for the system operated based on the frequency-to-power mapping technique. It can be seen from Fig. 3(a) that an ACF have different slopes at different RF signal frequencies. The smallest ACF slope occurs at around the midpoint of an ACF. Fig. 3(b) plots the ACFs when using a 2.43 km, 4.24 km and 9.5 km standard SMF as a dispersive medium. It can be seen from the figure that using a short SMF can obtain a large one-to-one-mapping frequency measurement range but the ACF slope is small. While it is preferable to have a short fibre to reduce the system size and loss, and to achieve a large frequency measurement range, a small ACF slope will lead to low frequency measurement resolution and large frequency measurement errors [8], [15], [16]. This can be seen from Fig. 4(a), which shows the errors at different frequencies caused by 0.1 dB error in the output RF signal power ratio measurement. The ACF, which is used to obtain the errors shown in Fig. 4(a), together with the ACF slope at different frequencies, are shown in Fig. 4(b). As shown, the frequency measurement error is large at the RF signal frequency of around 25 GHz where the ACF has a small slope. Fig. 5 shows the minimum slope in an ACF and the required standard SMF length for different frequency measurement ranges. The system with an

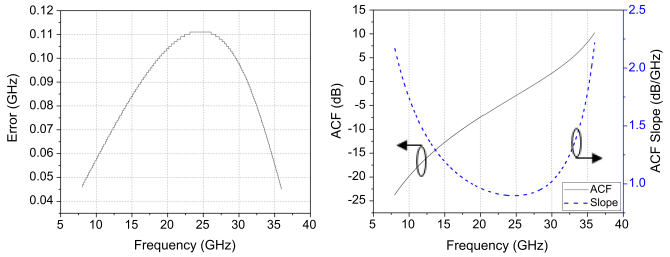

Fig. 4. (a) Frequency measurement errors caused by 0.1 dB output RF signal power ratio measurement errors. (b) ACF of the proposed frequency measurement system and the ACF slope at different frequencies.

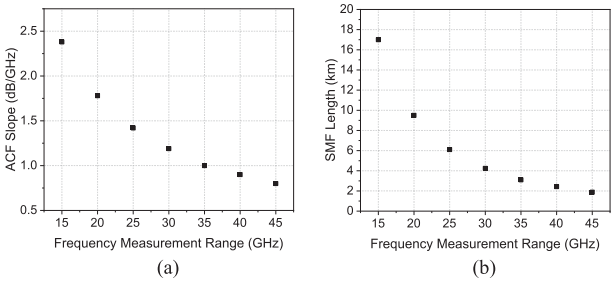

Fig. 5. (a) ACF slope at around the midpoint of an ACF and (b) required standard SMF length versus frequency measurement range.

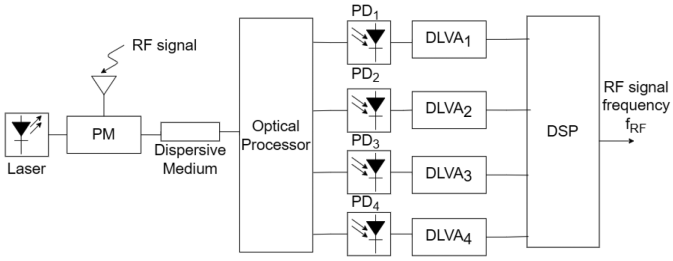

Fig. 6. Structure of the two-ACF based frequency measurement system.

around 40 GHz frequency measurement range needs a 2.43 km long standard SMF. The resultant ACF has a minimum slope of 0.9 dB/GHz at 24.8 GHz. Until now, all reported systems that use an ACF for instantaneous microwave frequency measurement have a trade-off between frequency measurement range and resolution [17].

III. System With Two ACFs for Improving Frequency Measurement Resolution

The proposed structure can be extended to produce two ACFs, which are designed to focus on measuring an RF signal frequency in a specified range with an improved frequency measurement resolution. Fig. 6 shows the structure of the two-ACF based frequency measurement system. In this case, the LCOS based optical processor produces four output optical signals, which have different optical carrier phase shifts α_N. Each of the four output optical signals is detected by a PD followed by a DLVA as in the basic structure shown in Fig. 1. Two ACFs

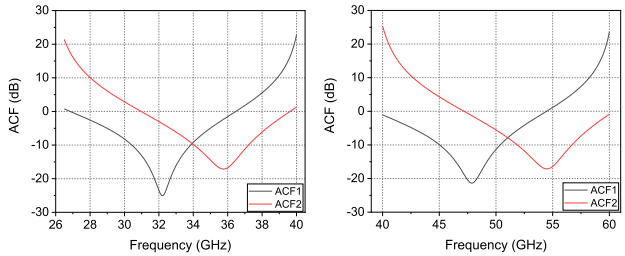

Fig. 7. ACF_1 and ACF_2 of the two-ACF based frequency measurement system. (a) The SMF length is $L = 6.5$ km and the phase shifts introduced to the optical carrier at the four optical processor outputs are $\alpha_1 = -26°$, $\alpha_2 = -116°$, $\alpha_3 = 190°$ and $\alpha_4 = 100°$. (b) The SMF length is $L = 2.8$ km and the phase shifts introduced to the optical carrier at the four optical processor outputs are $\alpha_1 = -34°$, $\alpha_2 = -124°$, $\alpha_3 = 190°$ and $\alpha_4 = 100°$.

(ACF_1 and ACF_2) are produced in the DSP based on two pairs of DLVA output DC voltages ($V_{o,DLVA1}$ and $V_{o,DLVA2}$, $V_{o,DLVA3}$ and $V_{o,DLVA4}$). They are given by

$$\begin{aligned} ACF_1(f_{RF}) &= \frac{V_{o,DLVA2} - V_{o,DLVA1}}{DLVA\ Slope} \\ &= 10\log_{10}\left[I_{RF,2}^2(f_{RF}) + I_{2RF,2}^2(f_{RF})\right] \\ &\quad - 10\log_{10}\left[I_{RF,1}^2(f_{RF}) + I_{2RF,1}^2(f_{RF})\right] \end{aligned} \tag{10}$$

$$\begin{aligned} ACF_2(f_{RF}) &= \frac{V_{o,DLVA4} - V_{o,DLVA3}}{DLVA\ Slope} \\ &= 10\log_{10}\left[I_{RF,4}^2(f_{RF}) + I_{2RF,4}^2(f_{RF})\right] \\ &\quad - 10\log_{10}\left[I_{RF,3}^2(f_{RF}) + I_{2RF,3}^2(f_{RF})\right] \end{aligned} \tag{11}$$

In addition to the subtraction and division operation, the DSP performs a comparison between the two ACF values. The ACF with a larger value is used to determine the input RF signal frequency via a look-up table as in the case of the one-ACF based frequency measurement system. Using two ACFs for frequency measurement allows a longer SMF to be used for estimating an RF signal frequency over a specified frequency range, which results in a higher frequency measurement resolution. For example, considering an application that requires measuring an RF signal frequency over the Ka band, i.e., 26.5–40 GHz. The SMF length and the four optical carrier phase shifts are designed to be $L = 6.5$ km and $\alpha_1 = -26°$, $\alpha_2 = -116°$, $\alpha_3 = 190°$ and $\alpha_4 = 100°$ respectively. Note that the two optical carrier phase shifts in each pair of the optical processor output ports that use to produce an ACF, have a 90° phase difference, so that the two ACFs shown in (10) and (11) behave as $\tan^2(\theta(f_{RF})\text{-}k)$ where $0° \leq k \leq 180°$ when the system is operated under small signal modulation condition. The two ACFs obtained using (10) and (11) together with the above system parameter values are plotted in Fig. 7(a). The figure shows the two ACFs have different values at different RF signal frequencies. The DSP compares the two ACF values and uses the ACF that has a larger value to estimate the RF signal frequency. According to Fig. 7(a), if the value of

ACF_1 is larger than that of ACF_2 then the frequency of the input RF signal must be in the range of 26.5–33.92 GHz. ACF_1, which has a one-to-one mapping between the ACF value and the RF signal frequency in this frequency range, will be used to obtain the RF signal frequency. On the other hand, if ACF_2 has a larger value than ACF_1 then the input RF signal frequency must be in the 33.92–40 GHz frequency range. In this case, the RF signal frequency is obtained by using ACF_2, which has a one-to-one ACF value and RF signal frequency mapping in this range. The smallest ACF slope in the two ACFs is 2.91 dB/GHz (at 31.1 GHz in ACF_1), which is over 3 times larger than the smallest ACF slope (0.9 dB/GHz) in the one-ACF scheme presented in Section II. Hence the two-ACF based frequency measurement system shown in Fig. 6 should have a higher resolution and smaller errors in a specified frequency measurement range, than the reported systems where the RF signal frequency is obtained by using one ACF. Fig. 7(b) shows, when the frequency measurement range changes to the U band, i.e., 40–60 GHz, the system parameters can be adjusted for the ACFs in the two-ACF based system to have over three-time improvement in slope compared to the one-ACF based system.

The proposed frequency measurement system has a simple structure as it is formed by a microwave photonic link composed of a laser source, an optical PM and a piece of fibre, and a signal processing and detection unit. The LCOS based optical processor, which is used to introduce phase shifts to the optical carriers, and the DSP, which is used to perform subtraction, division and comparison operations, are commercially available. Hence the proposed system can be constructed using off-the-shelf components. A PM has lower loss compared to a Mach Zehnder modulator (MZM), which is employed in most reported frequency measurement systems. A PM does not require a DC bias voltage, and hence the proposed structure has no bias drift problem and is suitable for use in remote antenna applications. The frequency measurement systems shown in Figs. 1 and 6 have a robust performance that is insensitive to environmental perturbations. On the other hand, the reported frequency measurement systems need accurate control on the light polarisation state [10], [11] and suffer from drift in the characteristic of the component such as a Mach Zehnder interferometer (MZI) [9] used for frequency measurement. Note that optical PMs with bandwidths of over 100 GHz have been reported [18] and photodetectors with 100 GHz bandwidths are commercially available [19]. The bandwidth of the proposed one-ACF and two-ACF based frequency measurement systems are only limited by the bandwidth of the DLVAs that are used to measure the system output RF signal powers. Commercial DLVAs, e.g., Minicircuits ZV47-K44+ power detector, have a bandwidth of 0.5 to 43.5 GHz. For applications that require measuring the frequency of an RF signal beyond 43.5 GHz, waveguide power sensors [20], which have bandwidths that cover 50 to 110 GHz, can be used instead of DLVAs for measuring the system output RF signal powers. Therefore, the proposed system can measure a very high RF signal frequency with an improved frequency measurement resolution. The response time of the proposed frequency measurement system is determined by the time delay of the optical signal travelled through the SMF. The simulation result in Fig. 7(a) shows a 6.5 km SMF is needed for measuring an RF signal frequency over the Ka band. This results in a time delay of 32.5 μs. Hence the latency of the proposed frequency-to-power-mapping based frequency measurement system is around 8 times better than the reported frequency-to-time-mapping based frequency measurement system [3].

Note that frequency measurement systems based on measuring a system output DC voltage have been reported [21], [22], [23]. They do not require DLVAs but they need an electrical power splitter to split the incoming RF signal into two portions. They have the advantages of compact structure and fast response time as they rely on the time delay between two RF signals rather than dispersion in a long SMF for frequency measurement. However, the input RF signal amplitude needs to be accurately measured prior to frequency measurement and the measurement errors can be 5% of the input RF signal frequency. A one-to-one mapping between the system output DC voltage and the input RF signal frequency is only demonstrated up to around 13 GHz [23].

IV. Experimental Results

Experiments were set up similar to Figs. 1 and 6 to demonstrate the concept of the proposed frequency measurement systems. The laser source was a tunable laser (Keysight N7711A). It generated a CW light with 1550.5 nm wavelength and 10 dBm optical power. The light was launched into a 20 GHz bandwidth PM (EOSpace PM-0S5-20-PFA-PFA). The phase modulated optical signal at the PM output passed through a length of standard SMF into an LCOS based optical processor (Finisar WaveShaper 4000A). The WaveShaper (WS) was programmed to introduce different phase shifts to the optical carriers at different WS output ports. An erbium-doped fibre amplifier (EDFA) was used to compensate for the system loss. The system output optical signals were detected by PDs (Discovery Semiconductor DSC30S).

Due to the lack of DLVAs, the proposed frequency measurement systems were demonstrated by using a vector network analyser (VNA) to measure the system output amplitude responses, as in most of the reported ACF based frequency measurement systems, e.g., [5], [6], [8]. The VNA available for experiment had a bandwidth of 50 kHz to 18 GHz. Since the WS had a limited resolution, the RF modulation sidebands need to be at least 8 GHz away from the optical carrier to avoid having effects after introducing a phase shift to the optical carrier. Therefore, due to the equipment limitation, the proposed frequency measurement system can only be demonstrated in the 8 to 18 GHz frequency range. According to Fig. 5(b), a SMF with a length of around 10 km is needed for 8–18 GHz RF signal frequency measurement in the basic one-ACF based frequency measurement system. Therefore, a 9.6 km long SMF was employed in the experiment. The WS was programmed to shift the phase of the optical carrier at the WS output Port 1 and 2 by $\alpha_1 = 0°$ and $\alpha_2 = -90°$ respectively. The optical signal from the WS output Port 1 was detected by the PD whose output was connected to the VNA. The amplitude responses of the system produced by the two WS output optical signals were used to obtain an ACF, which is

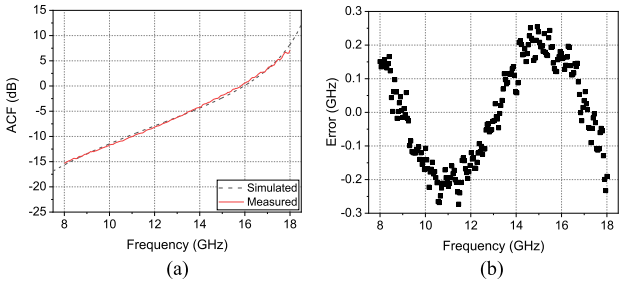

Fig. 8. (a) Measured (solid) and simulated (dashed) ACF of the proposed frequency measurement system designed to generate one ACF. (b) Frequency measurement errors obtained by comparing the measured and simulated ACFs.

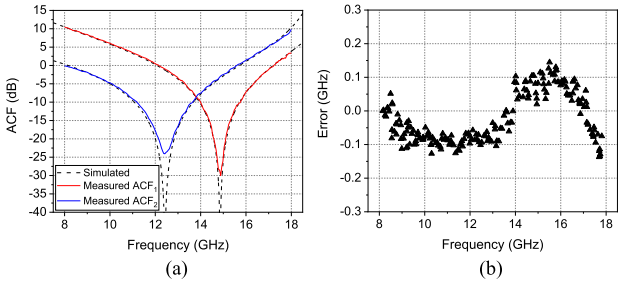

Fig. 9. (a) Measured (solid) and simulated (dashed) ACF of the proposed frequency measurement system designed to generate two ACFs. (b) Frequency measurement errors obtained by comparing the measured and simulated ACFs.

shown by the red solid line in Fig. 8(a). The figure also shows the simulated ACF. Frequency measurement errors can be obtained by comparing the measured and simulated ACFs, which are shown in Fig. 8(b). The results show the errors, when using one ACF for 8–18 GHz RF signal frequency measurement, are between −273 MHz to 255 MHz. These frequency measurement errors are similar to ±200 MHz and ±300 MHz errors in the reported one-ACF based frequency measurement systems [6], [13]. It can be seen from Fig. 8(b) that the measurement errors are not randomly distributed. This is because, as was stated in Section II, the ACF slope is different at different frequencies. The ACF shown in Fig. 8(a) has a small slope at 15 GHz and hence the measurement error is high at around this frequency. Note that, due to the presence of the higher order sidebands, the ACF is slightly different for different modulation indexes, which can be seen from the inset of Fig. 3(a). The simulated ACF shown in Fig. 8(a) was obtained using a constant 0.3 modulation index for different frequencies. However, in practice, the modulation index changes with the frequency because an optical modulator has a frequency dependent switching voltage. This results in a slight difference between the measured and simulated ACFs, and consequently frequency-dependent measurement errors. The errors can be reduced by ensuring the system is operated under small signal modulation condition and/or including the PM switching voltage frequency dependent characteristic into the simulated ACF.

Next, the 9.6 km SMF was replaced by a 20.4 km SMF to demonstrate the two-ACF based frequency measurement system. The phase shifts introduced to the optical carriers at the four WS output ports were designed to be $\alpha_1 = -89.6°$, $\alpha_2 = 0.4°$, $\alpha_3 = -117.2°$ and $\alpha_4 = -27.2°$. Two ACFs were obtained from the four system output amplitude responses measured on the VNA. Fig. 9(a) shows the two measured and simulated ACFs. Frequency measurement errors were obtained by comparing the measured and simulated ACF_1 in the 8–13.8 GHz range and comparing the measured and simulated ACF_2 in the 13.8–18 GHz range. Fig. 9(b) shows the errors are within ±150 MHz in the 8–18 GHz frequency measurement range. The experimental results verify errors can be reduced by using two ACFs, which have a steeper slope, for microwave frequency measurement, compared to the reported systems that use one ACF for microwave frequency measurement. Note that there are few reported photonics-based frequency measurement systems that can achieve below ±100 MHz measurement errors [24], [25], [26]. However, they all require an electrical hybrid coupler or a power splitter to split an RF signal into two portions. They have complex structures, e.g., the frequency measurement system presented in [24] consists of three laser sources with 80 nm wavelength difference, two optical modulators and three long spools of SMF. The frequency measurement systems presented in [25] and [26] rely on sweeping the frequency of a microwave source or a laser source. Hence, they are not instantaneous frequency measurement systems. Furthermore, these two frequency measurement systems use a specially designed component such as a Chalcogenide waveguide [25] or a microring resonator [26] to implement an optical notch filter. On the other hand, the proposed instantaneous frequency measurement system has a simple structure and can be constructed using off-the-shelf components.

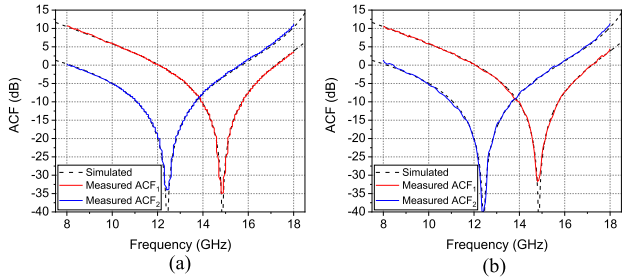

Fig. 10. Measured ACFs (solid lines) of the proposed frequency measurement system obtained in (a) the first day and (b) the second day. The system parameter settings are the same as that used to obtain the ACFs shown Fig. 9(a).

To investigate the repeatability and the robustness of the proposed frequency measurement system, the ACF measurements shown in Fig. 9(a) were repeated twice in two different days using the same system parameter setting. The measured ACFs, which are shown in Fig. 10(a) and 10(b), are very similar to that shown in Fig. 9(a). The frequency measurement errors obtained by comparing the measured and simulated ACFs are less than ±150 MHz. The proposed frequency measurement system output stability was also examined. This was done by applying a 15 GHz RF signal into the PM and measuring the PD output RF signal power using an electrical signal analyser (ESA) over a period of time for a carrier phase shift of −27.2°. Fig. 11(a)

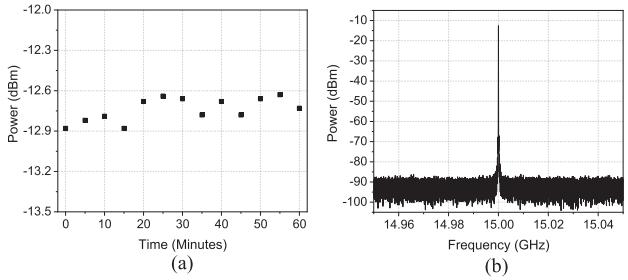

Fig. 11. (a) Measured system output RF signal powers. (b) System output electrical spectrum. The input RF signal frequency is 15 GHz and the phase shift introduced by the WS to the optical carrier is $-27.2°$.

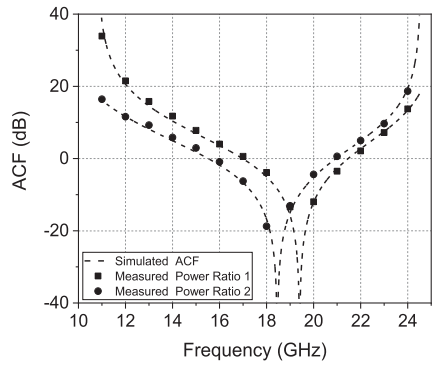

Fig. 12. Measured output RF signal power ratios and simulated ACFs of the proposed frequency measurement system designed to measure the frequency of an RF signal in an 11–24 GHz frequency measurement range. The phase shifts introduced to the optical carriers at the four WS output ports are $\alpha_1 = -62°$, $\alpha_2 = -152°$, $\alpha_3 = -50°$ and $\alpha_4 = -140°$.

shows there is less than 0.3 dB change in the output RF signal power during the one-hour measurement period. The measurements indicate that the proposed frequency measurement system has a stable and robust performance. Fig. 11(b) shows the system output electrical spectrum measured on the ESA connected to the PD output. The average optical power into the PD is 10 dBm and the ESA resolution bandwidth is 10 kHz. The noise floor of around -88 dBm shown in the figure is the ESA noise floor. This indicates that the noise floor of the proposed frequency measurement system is below -128 dBm/Hz. The figure also shows the system has a high signal-to-noise ratio (SNR) of over 70 dB for a noise bandwidth of 10 kHz.

The 20.4 km SMF was replaced by a 15.6 km SMF and the phase shifts introduced to the optical carriers by the optical processor were adjusted to demonstrate RF signal frequency measurement in an 11–24 GHz measurement range. Since the VNA available for experiment had a limited bandwidth of 18 GHz, the output RF signal power ratios for different input RF signal frequencies were measured on an ESA connected to the PD output. Fig. 12 shows the power ratios obtained at different input RF signal frequencies together with the two simulated ACFs. Close agreement between the experimental and simulation results can be seen. This demonstrates the proposed instantaneous frequency measurement system can be designed to measure an RF signal frequency in different frequency ranges.

V. Conclusion

A photonics-based instantaneous microwave frequency measurement system has been presented. The system is designed to produce two ACFs, which are used to determine an RF signal frequency over a specified frequency range. It has the advantages of higher frequency measurement resolution and smaller frequency measurement errors compared to the conventional one-ACF based frequency measurement systems. The proposed system can be constructed using off-the-shelf components, has a robust performance and is suitable for use in remote antenna applications. Experimental results demonstrate reduction of frequency measurement errors from ± 270 MHz to ± 150 MHz in the 8–18 GHz frequency measurement range, by using the proposed two-ACF based frequency measurement system.

References

[1] S. Hu, X. Han, P. Wu, Y. Gu, and M. Zhao, "A photonic technique for microwave frequency measurement employing tunable dispersive medium," in *Proc. Int. Topical Meeting Microw. Photon.*, 2011, pp. 165–168.

[2] S. T. Winnall, A. C. Lindsay, M. W. Austin, J. Canning, and A. Mitchell, "A microwave channelizer and spectroscope based on an integrated optical Bragg-grating Fabry-Perot and integrated hybrid Fresnel lens system," *IEEE Trans. Microw. Theory Tech.*, vol. 54, no. 2, pp. 868–872, Feb. 2006.

[3] T. A. Nguyen, E. H. W. Chan, and R. A. Minasian, "Photonic instantaneous multiple frequency measurement using a frequency shifting recirculating delay line structure," *J. Lightw. Technol.*, vol. 32, no. 20, pp. 3831–3838, 2014.

[4] L. Liu, W. Xue, and J. Yue, "Photonic approach for microwave frequency measurement using a silicon microring resonator," *IEEE Photon. Technol. Lett.*, vol. 31, no. 2, pp. 153–156, Jan. 2019.

[5] H. Wang, S. Zhang, X. Zou, Z. Zhang, Y. Zhang, and Y. Liu, "Photonic microwave frequency measurement based on frequency-configurable pilot tones," *IEEE Photon. Technol. Lett.*, vol. 30, no. 4, pp. 363–366, Feb. 2018.

[6] J. Li et al., "Photonic-assisted microwave frequency measurement with higher resolution and tunable range," *Opt. Lett.*, vol. 34, no. 6, pp. 743–745, 2009.

[7] L. Liu and W. Xue, "Instantaneous microwave frequency measurement based on two cascaded photonic crystal nanocavities," *IEEE Photon. J.*, vol. 12, no. 6, Dec. 2020, Art no. 4501809.

[8] Z. Zhao, K. Zhu, L. Lu, and C. Lu, "Instantaneous microwave frequency measurement using few-mode fiber-based microwave photonic filters," *Opt. Exp.*, vol. 28, no. 25, pp. 37353–37361, 2020.

[9] J. Dai et al., "A simple photonic-assisted microwave frequency measurement system based on MZI with tunable measurement range and high resolution," *IEEE Photon. Technol. Lett.*, vol. 22, no. 15, pp. 1162–1164, Aug. 2010.

[10] S. Pan and J. Yao, "Instantaneous microwave frequency measurement using a photonic microwave filter pair," *IEEE Photon. Technol. Lett.*, vol. 22, no. 19, pp. 1437–1439, Oct. 2010.

[11] Z. Tu, A. Wen, Y. Gao, W. Chen, Z. Peng, and M. Chen, "A photonic technique for instantaneous microwave frequency measurement utilizing a phase modulator," *IEEE Photon. Technol. Lett.*, vol. 28, no. 24, pp. 2795–2798, Dec. 2016.

[12] U. Gliese, S. Norskov, and T. N. Nielsen, "Chromatic dispersion in fiber-optic microwave and millimeter-wave links," *IEEE Trans. Microw. Theory Tech.*, vol. 44, no. 10, pp. 1716–1724, Oct. 1996.

[13] J. Zhou, S. Fu, S. Aditya, P. P. Shum, and C. Lin, "Instantaneous microwave frequency measurement using photonic technique," *IEEE Photon. Technol. Lett.*, vol. 21, no. 15, pp. 1069–1071, Aug. 2009.

[14] X. Zhang, H. Chi, X. Zhang, S. Zheng, X. Jin, and J. Yao, "Instantaneous microwave frequency measurement using an optical phase modulator," *IEEE Microw. Wireless Compon. Lett.*, vol. 19, no. 6, pp. 422–424, Jun. 2009.

[15] J. Zhou, S. Aditya, P. P. Shum, and J. Yao, "Instantaneous microwave frequency measurement using a photonic microwave filter with an infinite impulse response," *IEEE Photon. Technol. Lett.*, vol. 22, no. 10, pp. 682–684, May 2010.

[16] M. Pagani et al., "Low-error and broadband microwave frequency measurement in a silicon chip," *Optica*, vol. 2, no. 8, pp. 751–756, 2015.

[17] X. Zou and J. Yao, "An optical approach to microwave frequency measurement with adjustable measurement range and resolution," *IEEE Photon. Technol. Lett.*, vol. 20, no. 23, pp. 1989–1991, Dec. 2008.
[18] L. Alloatti et al., "100 GHz silicon–organic hybrid modulator," *Light Sci. Appl.*, vol. 3, no. 5, pp. 1–4, 2014.
[19] II-VI Incorporated, "XPDV412xRb 100 GHz photodetector datasheet," 2021. [Online]. Available: https://ii-vi.com/product-category/products/optical-communications/communication-components/high-speed-detectors-and-receivers/
[20] Keysight, "Waveguide power sensors," 2022. [Online]. Available: https://www.keysight.com/au/en/products/power-meters-power-sensors/waveguide-power-sensors.html
[21] N. Sarkhosh, H. Emami, L. Bui, and A. Mitchell, "Reduced cost photonic instantaneous frequency measurement system," *IEEE Photon. Technol. Lett.*, vol. 20, no. 18, pp. 1521–1523, Sep. 2008.
[22] N. Sarkhosh, H. Emami, L. Bui, and A. Mitchell, "Microwave photonic instantaneous frequency measurement with improved sensitivity," in *Proc. IEEE MTT-S Int. Microw. Symp. Dig.*, 2009, pp. 165–168.
[23] H. Emami, M. Hajihashemi, S. E. Alavi, A. S. M. Supaat, and L. Bui, "Microwave photonics instantaneous frequency measurement receiver based on a Sagnac loop," *Opt. Lett.*, vol. 43, no. 10, pp. 2233–2236, 2018.
[24] N. Shi, Y. Gu, J. Hu, Z. Kang, X. Han, and M. Zhao, "Photonic approach to broadband instantaneous microwave frequency measurement with improved accuracy," *Opt. Commun.*, vol. 328, pp. 87–90, 2014.
[25] H. Jiang et al., "Wide-range, high-precision multiple microwave frequency measurement using a chip-based photonic Brillouin filter," *Optica*, vol. 3, no. 1, pp. 30–34, 2016.
[26] S. Song, S. X. Chew, L. Nguyen, and X. Yi, "High-resolution microwave frequency measurement based on dynamic frequency-to-power mapping," *Opt. Exp.*, vol. 29, no. 26, pp. 42553–42568, 2021.